

# 1 Assessment of the aerosol optical depths measured by satellite- 2 based passive remote sensors in the Alberta oil sands region

3 Christopher E. Sioris<sup>1</sup>, Chris A. McLinden<sup>1</sup>, Mark W. Shephard<sup>1</sup>, Vitali E. Fioletov<sup>1</sup>, and Ihab  
4 Abboud<sup>1</sup>

5 [1] {Environment and Climate Change Canada (ECCC), Toronto, ON, Canada}

6 *Correspondence to:* Christopher E. Sioris (christopher.sioris@canada.ca)

7 **Abstract.** Several satellite aerosol optical depth (AOD) products are assessed in terms of their data quality in the  
8 Alberta oil sands region. The instruments consist of MODIS (Moderate resolution Imaging Spectroradiometer),  
9 POLDER (Polarization and Directionality of Earth Reflectances), MISR (Multi-angle Imaging SpectroRadiometer),  
10 and AATSR (Advanced Along-Track Scanning Radiometer). The AOD data products are examined in terms of  
11 multiplicative and additive biases determined using local AERONET (AEROCAN) stations. Correlation with  
12 ground-based data is used to assess whether the satellite-based AODs capture day-to-day, month-to-month, and  
13 spatial variability. The ability of the satellite AOD products to capture interannual variability is assessed at Albion  
14 Mine and Shell Muskeg River, two neighbouring sites in the northern mining region where a statistically significant  
15 positive trend (2002-2015) in PM<sub>2.5</sub> mass density exists. An increasing trend of similar amplitude (~5%/year) is  
16 observed in this northern mining region using some of the satellite AOD products.

## 17 1 Introduction

18 Fine-mode aerosols can be harmful to the respiratory system in large doses and are thus a critically important  
19 constituent with regard to air quality. For this reason, particulate matter with median aerodynamic diameter less than  
20 2.5 μm (PM<sub>2.5</sub>) is one of the atmospheric observables used to calculate the Air Quality Health Index (AQHI) in  
21 Canada (Stieb et al., 2008). Similar indices are used in other countries (Kelly et al., 2012). Tropospheric aerosols are  
22 also a major source of uncertainty in estimating the radiative forcing of climate (Myhre et al., 2013). Many satellite-  
23 based instruments can provide information about atmospheric aerosols in the form of aerosol optical depth (AOD), a  
24 measure of the vertically integrated extinction of the solar beam by aerosols. Measurements of AOD tend to be  
25 proportional to particulate matter mass density measured at the surface when the boundary layer aerosol  
26 concentrations are elevated (e.g. Tian and Chen, 2010).

27 The Alberta oil sands region (AOSR) has been under rapid industrial development during the past decade (Foote,  
28 2012). Satellite measurements already indicate a significant increasing trend in nitrogen dioxide between 2005 and  
29 2014 (McLinden et al., 2012; McLinden et al., 2016). Additionally, the AOSR is being deforested as part of  
30 expanding surface mining operations. This inevitably increases levels of dust, which partly arises from

1 transportation by trucks. Dust is one of many aerosol types of relevance in the AOSR. Other main aerosol types  
2 include organic aerosols, both natural and anthropogenic (Liggio et al., 2016), as well as ammonium sulfate.

3 Passive remote sensing of aerosol over land is challenging because, for a cloud-free scene, most of the nadir  
4 radiance is coming from direct reflection off the surface at visible wavelengths, not from aerosol scattering. This is  
5 particularly true for the AOSR, which consists of an irregularly-shaped industrial area to the south comprised of  
6 non-vegetated (cleared) mining locations and a second area to the north where mostly surface mining is occurring,  
7 as both areas have high surface albedo in the visible. Within the AOSR, the land type changes on spatial scales  
8 smaller than the typical  $10 \times 10$  km AOD footprint of a satellite-based instrument. Considering the area surrounding  
9 the AOSR, specifically the rectangular area between  $55.0$  and  $58.5^\circ\text{N}$  and  $114.0$  to  $108.5^\circ\text{W}$ , the land is covered by  
10 evergreen needleleaf forest (70%) and some deciduous broadleaf forest (23%), which is typical of the boreal forest  
11 in the northern portions of the Alberta and Saskatchewan.

## 12 **2 Method**

13 In order to study the spatiotemporal distribution of AOD in the AOSR, data from several satellite-based instruments  
14 are used. Satellite-based aerosol sensors are chosen based on a number of factors. One of the goals of the study is to  
15 examine long-term AOD trends, so preference is given to instruments with longer data records. Instruments that  
16 view a scene with multiple viewing angles were selected as the multi-angle capability is useful for disentangling the  
17 contributions to the scene reflectance by the surface and by the overlying aerosols (e.g. Bevan et al., 2012). Such  
18 instruments include Multi-angle Imaging Spectroradiometer (MISR) (Diner et al., 1989), the Polarization and  
19 Directionality of Earth Reflectances (POLDER) series (Deschamps et al, 1994) including POLDER/PARASOL  
20 (Polarization & Anisotropy of Reflectance for Atmospheric Sciences coupled with Observations from a Lidar), and  
21 the Along-Track Scanning Radiometer (ATSR) series (see Table 1 for the spatial resolution, temporal coverage and  
22 wavelength at which AOD is reported for each of the satellites). In addition, MODIS (Moderate resolution Imaging  
23 Spectroradiometer) is chosen partly because it has a long wavelength channel ( $2.1 \mu\text{m}$ ) that allows the surface  
24 reflectance to be accurately determined over vegetation without contamination from fine-mode aerosols (e.g.  
25 particles with radii of  $<0.2 \mu\text{m}$ ) by virtue of the correlation between visible and  $2.1 \mu\text{m}$  surface reflectance for  
26 vegetation (e.g. Kaufman et al., 2002; Li et al., 2005). MODIS/Aqua collection 6 data are used (see Appendix for  
27 providers and version numbers of other satellite data products). For MODIS, there are two AOD retrieval algorithms  
28 yielding the Dark Target (DT) (Levy et al., 2013) and the Deep Blue (DB) (Hsu et al., 2013) products. Specifically,  
29 the Corrected\_Optical\_Depth\_Land (550 nm) and the Deep\_Blue\_Aerosol\_Optical\_Depth\_550\_Land datasets were  
30 used and confidence for both datasets was extracted from the Quality\_Assurance\_Land dataset. The Dark Target  
31 algorithm exploits the fact that, for dark surfaces, aerosols tend to brighten the scene. For highly reflective surfaces  
32 such as snow in the visible spectral region, AOD cannot be retrieved using either the DT or DB approach. The  
33 MODIS Aqua DT product is also processed at 3 km spatial resolution in addition to the standard 10 km resolution  
34 available for both MODIS products (Levy et al., 2013). Each MODIS AOD measurement is assigned a confidence  
35 value. Confidence values of 1 and 0 indicate marginal and no confidence, respectively, while values of 2 and 3  
36 represent good and ideal confidence (Levy et al., 2013). For MODIS/Aqua collection 6, data with confidence  $\geq 1$  are

1 retained for validation. The theoretical basis of the MISR aerosol retrieval algorithm is given by Diner et al. (2008).  
2 The aerosol retrieval for AATSR is described by Bevan et al. (2012) and references therein. Deuzé et al. (2001)  
3 detail the approach used to retrieve aerosol information from POLDER observations over land.

4 MODIS Terra is not considered since it is highly similar to MODIS Aqua but, for collection 6, the former is less  
5 reliable for trend studies in spite of improvements relative to collection 5 (Levy et al., 2015). The MODIS-based  
6 Multiangle Implementation of Atmospheric Correction (MAIAC) (Lyapustin et al., 2011) product is not currently  
7 available in the AOSR (van Donkelaar et al., 2016). VIIRS (Visible Infrared Imaging Radiometer Suite) (Hillger et  
8 al., 2013) is not considered in this study because of its shorter data record relative to the MODIS sensors. Active  
9 remote sensing instruments are not considered because of the long revisit time and poor spatial coverage of the  
10 relatively small AOSR. The focus in this paper is primarily on the different aerosol sensors, rather than the different  
11 retrieval algorithms applied to the same satellite data (e.g. Popp et al., 2016), with the exception of the widely used  
12 Deep Blue and Dark Target algorithms for MODIS.

13 For validation of satellite-based AOD data, AERONET (Holben et al., 1998) is the ideal choice since the same  
14 quantity is measured by this ground-based network of direct-sun multiband photometers and the ~3 minute typical  
15 sampling interval generally ensures a good temporal coincidence during clear sky conditions. Quality-controlled  
16 AERONET data (Level 2, version 2) are used (<http://aeronet.gsfc.nasa.gov>). Cimel (French manufacturer) CE318  
17 sensors used by AERONET measure at several wavelength, some of them (e.g. 500 and 870 nm) are close to the  
18 wavelengths at which the selected satellite instruments report AOD (e.g. 470, ~550, and 865 nm). There are two  
19 AERONET sites in the oil sands region: Fort McMurray (56.752°N, 111.476°W) and Fort McKay (57.184°N,  
20 111.64°W). Measurements at Fort McMurray started in 2005. The Fort McKay site has only been in operation since  
21 August 2013 meaning that there is no temporal overlap with Advanced ATSR (AATSR) and only seven  
22 coincidences with POLDER/PARASOL using coincidence criteria of  $\pm 12$  minutes and 10 km. The spatial  
23 coincidence criterion corresponds to the smallest AOD footprints of the selected datasets (Table 1). A larger spatial  
24 coincidence criterion is not considered since, as shown below, strong spatial gradients in AOD exist in this aerosol  
25 source region. Furthermore, as mentioned in Sect. 1, the surface type also changes on such spatial scales. The  
26 temporal coincidence criterion was set to limit the number of independent AERONET measurements used in the  
27 statistical analysis. There can be multiple AERONET observations that are temporally coincident with a satellite  
28 observation and there can be up to four spatial coincident satellite AODs during a satellite overpass of an  
29 AERONET site. All of these coincidences are treated as independent data points in the validation and correlation  
30 analyses. In order to properly validate satellite AOD bias, AERONET 500 nm AODs are interpolated to the satellite  
31 AOD wavelengths (see Table 1) using the coincident AERONET Ångström exponent derived from 440 and 675 nm  
32 measurements, except for POLDER/PARASOL, for which no scaling of the AERONET AOD was applied.  
33 Since individual AERONET and satellite AODs are not normally distributed, we use linear least-squares weighted  
34 by Huber's function to determine the slope and offset since this is a robust regression method that does not  
35 completely disregard highly deviating points (Bergström and Edlund, 2014). The slope and offset values determined  
36 using Huber's weighting function are encompassed by the values obtained with seven alternative weighting

1 functions. Similarly, due the non-normal distribution of the individual AOD data, Spearman's rank correlation  
2 coefficient ( $r_s$ ) is chosen to study the site-specific AOD correlation based on individual AERONET-satellite  
3 coincidences.

4 The ability of each satellite-based sensor to capture the AOD seasonality in snow-free months is determined at Fort  
5 McMurray using Pearson's correlation of monthly averaged AODs (using all overlapping years) with AERONET. A  
6 minimum of 20 coincident data points per calendar month must be available for that month to be included in the  
7 correlation.

8 In order to assess the ability of the satellite data to capture the spatial variability in this region, the hourly in-situ  
9 surface-level  $PM_{2.5}$  from the 10 NAPS (National Air Pollution Surveillance) stations (Table 2) are used. Demerjian  
10 (2000) provided a review of the NAPS network, but since 2011, this network has undergone a gradual shift in the  
11 continuous monitoring of  $PM_{2.5}$  mass density from tapered element oscillating microbalances (TEOMs) to the  
12 SHARP (Synchronized Hybrid Ambient Real-time Particulate) monitoring system. The latter is a hybrid system,  
13 consisting of a nephelometer and a beta attenuation monitor (Hsu et al., 2016). The spatial correlation between  
14 median satellite AODs and NAPS  $PM_{2.5}$  mass densities is determined using coincident data. The use of medians  
15 rather than means reduces the sensitivity to outliers from forest fires. The same 10 km spatial coincidence criterion  
16 is used but temporal coincidence limit is extended to  $\pm 1$  hour to match the temporal resolution of the selected NAPS  
17 datasets.

18 Similar to the spatial and seasonal variability, the ability of the satellite instruments to capture interannual variability  
19 can be assessed by correlating yearly satellite-based AODs averaged over all coincidences with NAPS  $PM_{2.5}$   
20 measurements over the overlap period. 20 coincidences in a calendar year are required for the year to be included in  
21 the correlation calculation. As an example, for MISR, 14 sufficiently sampled years (2002-2015) are used in the  
22 correlation with NAPS data at Millennium mine.

23 For temporal trends, an ordinary least-squares simple linear regression is performed on relative anomalies derived  
24 from bias-corrected annual average and median AODs. The bias correction involves subtracting the AOD offset  
25 obtained through the validation with coincident Fort McMurray AERONET data. The mean of the yearly averages  
26 or medians is used to compute the relative anomalies. Similarly, for  $PM_{2.5}$ , the annual average of daily average  
27 values are used since the  $PM_{2.5}$  auto-correlation timescale is on the order of 6.5 hours, based on analysis of Albian  
28 mine  $PM_{2.5}$  data from 2002. The extra step of daily averaging prior to annual averaging yields more conservative  
29 annual standard error (s. e.) estimates. Partial years at the start and the end of a data record are removed. Trend  
30 periods are given below for each sensor. The area over which the satellite-based AOD trend maps are calculated is  
31  $0.1^\circ \times 0.1^\circ$  by default. This default setting is used to determine the AOD trend for both MODIS/Aqua 10 km products  
32 (2003-2015). The trend domain considered in this work spans from  $56-58^\circ N$  and  $111-112^\circ W$ . For sensors with  
33 poorer spatial coverage (MISR, AATSR, POLDER/PARASOL), the spatial binning is expanded in latitudinal and  
34 longitudinal increments of  $0.1^\circ$  until there are  $\geq 20$  observations in each calendar year within at least one grid cell in  
35 the domain. The trend maps are ultimately generated at  $0.3^\circ \times 0.3^\circ$  for AATSR (2003-2011) and MISR (2000-2015)  
36 whereas a  $0.4^\circ \times 0.4^\circ$  area is required for POLDER/PARASOL (2005-2013). Outlying individual datapoints ( $>4$

1 standard deviations above the climatological average in the domain) are recursively filtered mainly to reduce the  
2 influence of forest fires on trends. The same filtering is applied to the PM<sub>2.5</sub> datasets. Interannual consistency in the  
3 month-to-month sampling is checked for any location with a positive satellite AOD trend significant at the 95%  
4 confidence interval by calculating the average day-of-the-year for each calendar year. Such temporal sampling  
5 anomalies occur for MISR AOD data at some locations if a 0.1°×0.1° grid were used, for example. The Albian mine  
6 (2001-2008) and Shell Muskeg River (2009-2015) forest-fire-filtered PM<sub>2.5</sub> datasets were merged for trend analysis  
7 since the sensor was relocated from the former to the latter site in January 2009 and these sites are separated by <5  
8 km.

### 10 3 Results

11 First, the general spatial distribution of AOD is illustrated for some of the aforementioned data sets. In Fig. 1, the  
12 climatological average POLDER AOD on a 0.1° × 0.1° grid is shown. This is the default grid used for  
13 climatological maps of all satellite AOD datasets. The POLDER sample size per grid cell is 90 to 170 in the AOSR  
14 over the discontinuous period from 1996 to 2013 (see Table 1). There is a clear hotspot in 865 nm AOD in the  
15 AOSR region, roughly double the surrounding background values. Note that for POLDER and MISR, there are  
16 expected voids in their spatial coverage (Fig. 1) due to the spatial sampling of these instruments, whereas MODIS  
17 and AATSR footprints can be centered on any geolocation within the AOSR.

18 The AOD hotspot in the AOSR seen by POLDER is less obvious with MISR (Fig. 1). This is consistent with the  
19 relatively poorer ability of MISR to capture spatial variability based on spatial correlations of median AOD and  
20 PM<sub>2.5</sub> mass density over the ~10 available sites (Table 3). While the spatial correlation analysis relies on temporally  
21 coincident data, the less obvious AOD hotspot for MISR in Fig. 1 is also partly due to the spatiotemporal sampling  
22 by this instrument. Some locations are only sampled during a short period of the year, and thus the seasonal cycle of  
23 AOD is aliased into the MISR spatial distribution. Table 4 provides the number of coincidences for each satellite  
24 with the both Fort McMurray and Fort McKay AERONET observations to provide a sense of how the coincident  
25 sample sizes vary as a function of the satellite AOD data product.

26 The climatological AOD maps for the MODIS/Aqua collection 6 DT and DB products (2002-2014) are also shown  
27 in Fig. 1 however there is a major issue with the confidence as shown in Fig. 2. Near the Syncrude facility at  
28 Mildred Lake (57.05°N, 111.6°W), the confidence approaches 0 in both MODIS products in the two adjacent  
29 0.1°×0.1° cells (Fig. 2). In the western cell, the inadequate confidence in MODIS Aqua collection 6 DT data is due  
30 to failure of the AOD retrieval algorithm due to the 2.1 μm reflectance exceeding the allowed upper limit of 0.35.  
31 This is a fundamental limitation of the Dark Target retrieval strategy (see sect. 2). In the adjacent eastern cell, the  
32 low confidence stems from the low number of 0.5×0.5 km<sup>2</sup> pixels (see Table 1) used in the AOD retrieval. The  
33 number of pixels used in the AOD retrieval is reduced by the inland water mask (Carroll et al., 2016), the high 2.1  
34 μm reflectance (>0.35), but also by cloud masking and an independent test for optically thicker cirrus, diagnosed  
35 using the 1.38 μm channel (Levy et al., 2013; Hubanks, 2015). The high reflectance in the near-infrared affecting

1 the western cell and possibly the eastern cell is typical of desert or sandy loam. The higher spatial resolution of the  
2 MODIS-Aqua 3 km DT data clarifies the importance of this issue: key areas in the AOSR are simply not monitored  
3 with confidence by the current MODIS/Aqua DT product. For example, there are  $0.01^\circ \times 0.01^\circ$  areas with no AOD  
4 measurements of the highest confidence in 12 years, whereas surrounding, equal areas have tens of observations.  
5 The lack of confidence is not unique to the AOSR. Low confidence is also observed in urban areas within the  
6 province (e.g. Calgary, not shown). The low confidence in the MODIS DB product is due to the spatial  
7 heterogeneity of the surface between vegetated and non-vegetated area, which leads to pixels falsely identified as  
8 cloudy (N. Christina Hsu, NASA, priv. communication). Li et al. (2009) identified the need for improved AOD  
9 measurements using the DB algorithm over transitional land covers.

10 A similar issue exists for AATSR (Fig. 3) and ATSR-2 (not shown), which both have an exceedingly small number  
11 of successful retrievals in a  $0.1^\circ \times 0.1^\circ$  area containing the Mildred Lake Syncrude facility (e.g.  $N < 10$ ) during their  
12 respective missions (Table 1). Similarly to MODIS, this is probably caused by falsely identifying bright patches in  
13 otherwise vegetated scenes as clouds (P. North, Swansea University, priv. communication). Cloud fraction for  
14 successful AOD retrievals tends to be as high as 0.18 within the oil sands region, including the northern mining  
15 region, yet drops to 0.02 in the surrounding region (Fig. 3). Note that cloudy  $1 \times 1 \text{ km}^2$  pixels are not used during the  
16 AATSR AOD retrieval. The spatial correlation coefficient between sample size and cloud fraction as illustrated in  
17 Fig. 3 is -0.73, indicating that the spatial variation in AATSR sample size is mostly related to cloud flagging.  
18 Neither POLDER nor MISR show a sampling void in the AOSR. Table 1 shows that these two sensor types have  
19 coarser AOD spatial resolution by a factor of 3-4 than MODIS, ATSR-2, and AATSR. Note that some of the  $\text{PM}_{2.5}$   
20 sites are located in the periphery of the industrial and mining areas and thus spatial coincidences exist for MODIS  
21 and AATSR in spite of the aforementioned issues, given the 10 km coincidence criterion.

22 In terms of the validation using AERONET data (Table 4), MISR has a multiplicative bias (i.e. slope significantly  
23 less than unity), which is similar at both sites in the AOSR. The slope is of a similar value to the slope found in  
24 previous studies for inland (Liu et al., 2004), dusty (Kahn et al., 2005), and urban environments (Jiang et al., 2007).  
25 MODIS DB tends to yield more data than the DT product, but the correlation is lower with AERONET on  
26 individual coincidences and in terms of the seasonal variation. At the Fort McMurray AERONET sites, the MODIS  
27 products behave oppositely in terms of multiplicative and additive biases (discussed in Sect. 4). AATSR and  
28 POLDER/PARASOL have no major validation shortcomings.

### 29 **3.1 Trends**

30 Before considering trends in the AOSR, it is useful to look at whether the different satellite data products capture the  
31 AOD interannual variability at Fort McMurray, where a sufficiently long record (2005-2015) of 500 nm AOD  
32 exists. All of the products capture the interannual variability of the annual mean AOD observed by AERONET at  
33 Fort McMurray (Table 5). Correlation coefficients for forest-fire-filtered annual means tend to be only slightly  
34 lower.

1 In general, very few of the 200 grid cells in the trend domain (56-58°N, 111-112°W) indicate a statistically  
2 significant (2 s. e.) positive trend that is consistent from one satellite to the next. In fact, there are no points in the  
3 domain for which MODIS/Aqua DT (2003-2013), AATSR, or ATSR-2 (1996-2002, 0.3°×0.3°) show a significant  
4 positive trend in AOD. Similarly, POLDER/PARASOL only shows a significant positive trend in three adjacent grid  
5 points at 57.3°N between 111.3 and 111.5°W (see Fig. 4) and MISR also finds a significant positive trend at only  
6 two locations in the domain. Finally, MODIS/Aqua DB has two points with the largest and most significant positive  
7 AOD trend in the region of the Muskeg River mine at 57.25°N, 111.25°W (Fig. 4). In fact, two satellite data  
8 products, namely POLDER/PARASOL and MODIS/Aqua DB, exhibit a statistically significant positive trend in  
9 this mining area. Although not statistically different from zero, the AOD trend in both AATSR and MISR data is  
10 positive in the area of the positive POLDER/PARASOL trend (Fig. 4), whereas MODIS DT tends to show an  
11 insignificant negative trend.

12 Changes to the surface may be at the root of the increasing AOD trend in this area, either since clearing of  
13 vegetation could lead to higher concentrations of dust, or by biasing the AOD retrieval. Trends in surface albedo  
14 were determined from the combined MODIS Terra/Aqua MCD43C3 albedo data product at four wavelengths  
15 relevant to the MODIS or POLDER AOD retrievals: 470, 645, 860, and 2130 nm (see Appendix A). For all four  
16 wavelengths, neither the largest nor the most significant trends in surface reflectivity occur at 57.25°N, 111.25°W  
17 (not shown), where the largest and most significant MODIS DB AOD trend occurs and also within the larger area of  
18 the spatially coherent POLDER/PARASOL AOD trend.

19 Since aerosol optical depth histograms indicate a skewed distribution, it is useful to verify trends using annual  
20 medians. A significant positive trend of  $(4.1 \pm 1.1)\%/year$  ( $\pm 1$  standard error) (Figs. 5-6) and  $(5.7 \pm 1.6)\%/year$  is  
21 detected in the Albian mine/ Shell Muskeg River merged annual average and median  $PM_{2.5}$  mass densities (2002-  
22 2015), respectively. Limiting the merged  $PM_{2.5}$  dataset to the warm season (April-October) to mimic the temporal  
23 coverage of the satellite data (Table 4), the relative trend using annual averages is  $(4.6 \pm 1.2)\%/year$ , which is not  
24 change significantly from the trend using year-round data (Fig. 6). A consistent trend of  $(4.8 \pm 2.1)\%/year$  is found in  
25 annually-averaged  $PM_{2.5}$  at Albian mine (2002-2008) alone, and the trend there during the warm season is  
26  $(4.3 \pm 1.1)\%/year$ , also statistically significant and not different from the year-round trend. Furthermore, there is no  
27 indication of a discontinuity between 2008 and 2009 when the monitoring site was relocated. The relative trend in  
28  $PM_{2.5}$  at the surface is in quantitative agreement with the relative trends derived from MODIS/Aqua Deep Blue and  
29 POLDER/PARASOL annually averaged AOD data over similar, yet shorter periods. For both MODIS/Aqua Deep  
30 Blue and POLDER/PARASOL, trends using annual medians agree with trends determined using annual averages  
31 within their respective standard errors (1 s. e.). The low bias of POLDER/PARASOL AOD near these two Shell  
32 mines is expected from the validation with AERONET at Fort McMurray (Table 4) and previous work on larger  
33 spatial scales (Deuzé et al., 2001).

34 Contrary to the localized, significant AOD trend in satellite data records in the eastern portion of the Muskeg River  
35 region, a statistically significant trend is found at two other ground-based stations within the AOSR for the period  
36 2002-2014, namely Syncrude UE1 and Millennium mine (Fig. 6). The largest trend occurs at Millennium mine, the

1 closest NAPS station to the southeast of the Shell Muskeg River region (see Table 2 and Fig. 4 for location). The  
2 trend is insignificant using either annual means or median  $PM_{2.5}$  data at CNRL Horizon and Anzac where data  
3 records are shorter, while the trend at Wapasu (2013-2015) was not evaluated. The  $PM_{2.5}$  trends at the remaining  
4 sites in the AOSR, namely two sites at Fort McMurray and one at Fort McKay are discussed below. Note that  
5 POLDER/PARASOL does not measure at Syncrude UE1 (see Table 3) and there is insufficient sampling at  
6 Millennium Mine over an area of  $0.4^\circ \times 0.4^\circ$  in each of the years (2005-2013) for trend analysis. For  
7 POLDER/PARASOL, the trend, while mostly insignificant in the AOSR, is always positive. For AATSR, the AOSR  
8 has regions of statistically insignificant negative and positive trends. For MISR, the trend is positive in 56% of the  
9 trend domain and even more so (83%) in the northern half of the domain ( $57-58^\circ N$ ). For MODIS DB and DT, some  
10 of the AOSR is not sufficiently sampled with high confidence (see Sect. 2), but where confidence is  $\geq 1$ , the trend  
11 tends to be negative in 69% and 77% of this area, respectively. The calibration of the MODIS reflective solar bands  
12 is achieved by calibration with the solar diffuser. Some negative drift in AOD (Levy et al., 2015) is expected for  
13 MODIS Aqua similar to its Terra counterpart (see Sect. 2) as the designs of the solar diffuser and its stability  
14 monitor are nearly identical in the two MODIS sensors (Wu et al., 2013). Li et al. (2016) find a small positive trend  
15 in AOD over Athabasca ( $56-58^\circ N$ ,  $110-113^\circ W$ ) using MODIS/Aqua DB data (2004-2015), insignificant at the 2 s.e.  
16 level. Bari and Kindzierski (2016) found no indications of a positive trend in  $PM_{2.5}$  at Fort McKay and the Fort  
17 McMurray Athabasca Valley site, using a longer period (1998-2014), although, as shown in Fig. 2 of Bari and  
18 Kindzierski (2016) for Fort McKay, there is an abrupt decrease in  $PM_{2.5}$  mass densities that occurs between 2001  
19 and 2002 that has a profound effect on the trend and its uncertainty. This discontinuity is observed at all sites in the  
20 AOSR that extend back to 2001. An earlier study by the same authors (2015) also indicated no trend between 1998-  
21 2012 at the same sites and at the Fort McMurray Patricia MacInnes site as well.

#### 22 **4 Discussion and conclusions**

23 In this section, the advantages and limitations of the various data products are summarized. As shown in Table 4, all  
24 of the satellite sensors capture the temporal variability in AOD over Fort McMurray, based on correlations with  
25 AERONET, in spite of the low AODs there (e.g. Fig. 1). This temporal variability is largely driven by day-to-day  
26 variability as forest fires lead to episodes with large AODs ( $>3$ ) in summer months that strongly influence the  
27 calculated correlation.

28 The two MODIS AOD data products (Deep Blue and Dark Target) have low confidence in the AOSR partly due to  
29 issues relating to elevated surface reflectivity in the vicinity of the Mildred Lake Syncrude facility. However, the  
30 MODIS dark target product is the best at capturing temporal variability in terms of the correlation with individual  
31 AERONET AODs at Fort McMurray and in terms of capturing the month-to-month variability. Stronger short-term  
32 correlation with AERONET AODs reflects the superior spatial resolution of the MODIS radiances (Table 1), which  
33 is useful for resolving and filtering small clouds and localized areas of high surface reflectivity. Focussing on Fort  
34 McMurray, where there is a longer AERONET data record than at Fort McKay, MODIS DT has a slope greater than  
35 unity, in contrast to MODIS DB (Table 4). The same pattern of high and low slope values for the MODIS Aqua DT  
36 and DB (collection 6) products, respectively, was found over two sites in Pakistan, namely Lahore and Karachi, by



1 Bilal et al. (2016) and during non-fire summertime periods over semi-arid Nevada and California as shown in Table  
2 4 of the work of Loría-Salazar et al. (2016). A high slope may be related to the use of the 2.1  $\mu\text{m}$  channel to  
3 determine the reflectivity in the visible over non-vegetated surfaces as suggested by Bilal et al. (2016). High-biased  
4 AODs result because the surface reflectance in the visible assumed by the retrieval algorithm is less than the actual  
5 value as the relationship between the visible and 2.1  $\mu\text{m}$  was developed for vegetated land for which a stronger  
6 spectral variation exists than for barren land. Li et al. (2005) have shown that the spectral reflectance relationship is  
7 much different even for dry vegetation than green vegetation. Note that high day-to-day variability can be captured  
8 in spite of biases in assumed surface reflectance since the latter changes slowly with time over the warm season,  
9 when successful measurements occur more frequently. A MODIS algorithm designed to function over  
10 inhomogeneous surfaces such as the AOSR region, and which would also likely be applicable to urban areas, is  
11 being investigated to exploit the many benefits of MODIS radiance data. One such benefit is the twice-daily revisit  
12 over the AOSR that the current multi-angle sensors, namely MISR and SLSTR (Sea and Land Surface Temperature  
13 Radiometer) (Coppo et al., 2010), cannot offer. SLSTR, onboard the recently launched Sentinel-3a satellite, is the  
14 next generation in the ATSR series.

15 MISR clearly captures the short-term and month-to-month AOD variability at Fort McMurray based on correlations  
16 at the individual coincidence level and the monthly time scale (Table 4), but struggles to capture the local spatial  
17 variability including the AOD hotspot in the AOSR as discussed in Sect. 3. The MISR low bias may be related to the  
18 need for darker spherical particles (Kahn et al., 2010) given that forest fire smoke plays a significant role throughout  
19 western Canada in the warm season (O'Neill et al., 2002). Spherical particles with lower single scattering albedo  
20 (SSA) may also be required to properly represent local anthropogenic pollution (Kahn et al., 2010) in the AOSR.  
21 The  $3\times 3$  superpixel averaging that is used when the MISR retrieval fails for the central superpixel could also  
22 contribute to a low bias (Jiang et al., 2007), particularly at Fort McKay as background AODs to the west could be  
23 lowering the average.

24 AATSR has a major spatial sampling issue in the heart of the AOSR, but also captures month-to-month variability  
25 from late spring to early autumn (Table 4) as well as short-term (Table 4) and spatial variability (Table 3). Based on  
26 a previous analysis (Che et al., 2016), the AATSR AOD underestimation of the Swansea University product (also  
27 used here) is larger over barren surfaces or sparse vegetation. Such land cover types are present in the AOSR.

28 POLDER has a known negative offset in AOD (Deuzé et al., 2001), confirmed using coincident Fort McMurray  
29 AERONET AOD data. For the temporal trend calculation, the approach of using relative anomalies based on bias-  
30 corrected AODs is particularly important for POLDER/PARASOL because the very low 865 nm AODs (Fig. 1) and  
31 the negative offset (Table 4) do not allow a relative trend to be meaningful without bias correction. Nevertheless,  
32 POLDER/PARASOL is among the most accurate satellite-based aerosol sensor at Fort McMurray during periods  
33 of the higher AODs (e.g.  $\geq 0.4$ , Table 4), when its negative offset becomes rather trivial. Overall, the POLDER AOD  
34 product is without a major weakness relative to the other instruments, although it is provided at a relatively coarse  
35 spatial resolution (Table 1) and the fixed spatial sampling pattern of this sensor inhibits the application of spatial  
36 oversampling techniques. The use of polarized radiances reduces the sensitivity of the retrieved AOD to surface

1 reflectance (e.g. Deuzé et al., 2001). The trend in POLDER/PARASOL AOD at the Shell mines (Albian and Shell  
2 Muskeg River) is probably not driven by a trend in surface reflectance since agreement with AERONET tends to be  
3 independent of surface type (e.g. Chen et al., 2015). A future sensor of POLDER heritage, namely the Multi-  
4 viewing, Multi-channel, Multi-polarisation Imager (3MI), offers higher spatial resolution, the availability of longer  
5 wavelength channels, and the potential for accurate monitoring of the local aerosol loading in the decade to come.

6 While AODs in the AOSR are relatively small according to POLDER/PARASOL (Fig. 1), the significantly positive  
7 trend in AOD from this satellite sensor and the similar trend in observed surface-level PM<sub>2.5</sub> in the region of the  
8 Muskeg River mine points to the need to continue monitoring of this region with a combination of surface and  
9 satellite-based aerosol observations.

10 *Acknowledgements.* Helpful discussions with Shailesh Kharol (ECCC) on the size range of dust particles are  
11 gratefully acknowledged. The European Space Agency Climate Change Initiative program is acknowledged. Peter  
12 North (Swansea University) is thanked for comments on an earlier version of the manuscript.

## 13 **5 References**

14 Bari, M., and Kindzierski, W. B.: Fifteen-year trends in criteria air pollutants in oil sands communities of Alberta,  
15 Canada, *Environment International*, 74, 200–208, 2015.

16 Bari, M. A., and Kindzierski, W. B.: Evaluation of air quality indicators in Alberta, Canada – An international  
17 perspective, *Environment International*, 92-93, 119-129, 2016.

18 Bergström, P., and Edlund, O.: Robust registration of point sets using iteratively reweighted least squares, *Comput.*  
19 *Optim. Appl.*, 58, 543–561, 2014.

20 Bevan, S. L., North, P. R. J., Los, S. O., Grey, W. M. F.: A global dataset of atmospheric aerosol optical depth and  
21 surface reflectance from AATSR, *Remote Sens. Environ.*, 116, 199–210, 2012.

22 Bilal, M., Nichol, J. E., and Nazeer, M.: Validation of Aqua-MODIS C051 and C006 operational aerosol products  
23 using AERONET measurements over Pakistan, *IEEE J. Selected Topics Appl. Earth Observations Remote Sens.*, 9,  
24 2074-2080, 2016.

25 Bréon, F. M.: *Parasol Level-2 product data format and user manual*, Ed. 1 – Rev. 6, 2011.

26 Carroll, M. L., DiMiceli, C. M., Townshend, J. R. G., Sohlberg, R. A., Elders, A. I., Devadiga, S., Sayer, A. M., and  
27 R. C. Levy, R. C.: Development of an operational land water mask for MODIS Collection 6, and influence on  
28 downstream data products, *Int. J. Digital Earth*, doi: 10.1080/17538947.2016.1232756, 2016.

29 Chen, H., Cheng, T., Gu, X., Li, Z., and Wu, Y.: Evaluation of polarized remote sensing of aerosol optical thickness  
30 retrieval over China, *Remote Sens.*, 7, 13711-13728, doi:10.3390/rs71013711, 2015.

31 Coppo, P., Ricciarelli, B., Brandani, F., Delderfield, J., Ferlet, M., Mutlow, C., Munro, G., Nightingale, T., Smith,  
32 D., Bianchi, S., Nicol, P., Kirschstein, S., Hennig, T., Engel, W., Frerick, J., and J. Nieke: SLSTR: a high accuracy

1 dual scan temperature radiometer for sea and land surface monitoring from space, *J. Modern Opt.*, 57(18), 1815-  
2 1830, doi:10.1080/09500340.2010.503010.

3 Demerjian, K. L.: A review of national monitoring networks in North America, *Atmos. Environ.*, 34, 1861-1884,  
4 2000.

5 Deschamps, P.-Y., Bréon, F.-M., Leroy, M., Podaire, A., Bricaud, A., Buriez, J.-C., and Sèze, G.: The POLDER  
6 mission: Instrument characteristics and scientific objectives, *IEEE Trans. Geosci. Remote Sens.*, 32(3), 598-615,  
7 1994.

8 Deuzé, J. L., Bréon, F. M., Devaux, C., Goloub, P., Herman, M., Lafrance, B., Maignan, F., Marchand, A., Nadal,  
9 F., Perry, G., and Tanré, D.: Remote sensing of aerosols over land surfaces from POLDER-ADEOS-1 polarized  
10 measurements, *J. Geophys. Res.*, 106, 4913–4926, 2001.

11 Diner, D. J., Bruegge, C. J., Martonchik, J. V., Ackerman, T. P., Davies, R., Gerstl, S. A. W., Gordon, H. R., Sellers,  
12 P. J., Clark, J., Daniels, J. A., Danielson, E. D., Duval, V. G., Klassen, K. P., Lilienthal, G. W., Nakamoto, D. I.,  
13 Pagano, R., and Reilly, T. H.: MISR: A Multi-angle Imaging SpectroRadiometer for geophysical and climatological  
14 research from Eos. *IEEE Trans. Geoscience and Remote Sens.*, 27 (2), 200-214, 1989.

15 Diner, D. J., Abdou, W. A., Ackerman, T. P., Crean, K., Gordon, H. R., Kahn, R. A., Martonchik, J. V.,  
16 McMuldloch, S., Paradise, S. R., Pinty, B., Verstraete, M. M., Wang, M., and West, R. A.: Multi-angle Imaging  
17 SpectroRadiometer Level 2 aerosol retrieval algorithm theoretical basis, Revision G, JPL D-11400, Jet Propulsion  
18 Laboratory, California Institute of Technology, 2008.

19 Foote, L.: Threshold considerations and wetland reclamation in Alberta's mineable oil sands, *Ecology and Society*,  
20 17(1), 35, 2012.

21 Hillger, D., Kopp, T., Lee, T., Lindsey, D., Seaman, C., Miller, S., Solbrig, J., Kidder, S., Bachmeier, S., Jasmin, T.,  
22 and Rink, T.: First-light imagery from Suomi NPP VIIRS, *Bull. Amer. Meteor. Soc.*, 94, 1019-1029, 2013.

23 Holben, B., Eck, T., Slutsker, I., Tanre, D., Buis, J. P., Setzer, A., Vermote, E., Reagan, J. A., Kaufman, Y. J.,  
24 Nakajima, T., Lavenu, F., Jankowiak, I., and Smirnov, A.: AERONET – A federated instrument network and data  
25 archive for aerosol characterization, *Remote Sens. Environ.*, 66, 1–16, 1998.

26 Hsu, N. C., Jeong, M.-J., Bettenhausen, C., Sayer, A. M., Hansell, R., Seftor, C. S., Huang, J., and Tsay, S.-C.:  
27 Enhanced Deep Blue aerosol retrieval algorithm: The second generation, *J. Geophys. Res. Atmos.*, 118, 9296–9315,  
28 doi:10.1002/jgrd.50712, 2013.

29 Hsu, Y.-M., Wang, X., Chow, J. C., Watson, J. G., and Percy, K. E.: Collocated comparisons of continuous and  
30 filter-based PM<sub>2.5</sub> measurements at Fort McMurray, Alberta, Canada, *J. Air Waste Manage. Assoc.*, 66, 329-339,  
31 2016.

32 Hubanks, P.: MODIS atmosphere QA plan for Collection 006, Greenbelt, MD, USA, NASA Goddard Space Flight  
33 Center, version 8, 2015.

1 Jiang, X., Liu, Y., Yu, B., and Jiang, M.: Comparison of MISR aerosol optical thickness with AERONET  
2 measurements in Beijing metropolitan area, *Remote Sens. Environ.*, 107, 45–53, 2007.

3 Kahn, R. A., Gaitley, B. J., Martonchik, J. V., Diner, D. J., Crean, K. A., and Holben, B.: Multiangle Imaging  
4 Spectroradiometer (MISR) global aerosol optical depth validation based on 2 years of coincident Aerosol Robotic  
5 Network (AERONET) observations, *J. Geophys. Res.*, 110, D10S04, doi:10.1029/2004JD004706, 2005.

6 Kahn, R. A., Gaitley, B. J., Garay, M. J., Diner, D. J., Eck, T. F., Smirnov, A., and Holben, B. N.: Multiangle  
7 Imaging Spectroradiometer global aerosol product assessment by comparison with the Aerosol Robotic Network, *J.*  
8 *Geophys. Res.*, 115, D23209, doi:10.1029/2010JD014601, 2010.

9 Kaufman, Y. J., Tanré, D., and Boucher, O.: A satellite view of aerosols in the climate system, *Nature*, 419, 215-  
10 223, 2002.

11 Kelly, F. J., Fuller, G. W., Walton, H. A., and Fussler, J. C.: Monitoring air pollution: Use of early warning systems  
12 for public health, *Respirology*, 17, 7-19, 2012.

13 Levy, R. C., Mattoo, S., Munchak, L. A., Remer, L. A., Sayer, A. M., Patadia, F., and Hsu, N. C.: The Collection 6  
14 MODIS aerosol products over land and ocean, *Atmos. Meas. Tech.*, 6, 2989–3034, 2013.

15 Levy, R. C., Munchak, L. A., Mattoo, S., Patadia, F., Remer, L. A., and Holz, R. E.: Towards a long-term global  
16 aerosol optical depth record: applying a consistent aerosol retrieval algorithm to MODIS and VIIRS-observed  
17 reflectance, *Atmos. Meas. Tech.*, 8, 4083–4110, 2015.

18 Li, R.-R., Remer, L., Kaufman, Y. J., Mattoo, S., Gao, B.-C., and Vermote, E.: Snow and ice mask for the MODIS  
19 aerosol products, *IEEE Geosci. Remote Sens. Lett.*, 2, 306-310, 2005.

20 Li, Z., Zhao, X., Kahn, R., Mishchenko, M., Remer, L., Lee, K.-H., Wang, M., Laszlo, I., Nakajima, T., and Maring,  
21 H.: Uncertainties in satellite remote sensing of aerosols and impact on monitoring its long-term trend: a review and  
22 perspective, *Ann. Geophys.*, 27, 2755–2770, 2009.

23 Li, C., Hsu, N. C., Sayer, A. M., Krotkov, N. A., Fu, J. S., Lamsal, L. N., Lee, J., Tsay, S.-C.: Satellite observation  
24 of pollutant emissions from gas flaring activities near the Arctic, *Atmos. Environ.*, 133, 1-11, 2016.

25 Liggio, J., Li, S.-M., Hayden, K., Taha, Y. M., Stroud, C., Darlington, A., Drollette, B. D., Gordon, M., Lee, P., Liu,  
26 P., Leithead, A., Moussa, S. G., Wang, D., O'Brien, J., Mittermeier, R. L., Brook, J., Lu, G., Staebler, R., Han, Y.,  
27 Tokarek, T. T., Osthoff, H. D., Makar, P. A., Zhang, J., Plata, D., Gentner, D. R.: Oil sands operations are a major  
28 source of secondary organic aerosols, *Nature*, 534, 91-94, 2016.

29 Liu, Y., Sarnat, J. A., Coull, B. A., Koutrakis, P., and Jacob, D. J.: Validation of Multiangle Imaging  
30 Spectroradiometer (MISR) aerosol optical thickness measurements using Aerosol Robotic Network (AERONET)  
31 observations over the contiguous United States, *J. Geophys. Res.*, 109, D06205, doi:10.1029/2003JD003981, 2004.

1 Loría-Salazar, S. M., Holmes, H. A., Arnott, W. P., Barnard, J. C., Moosmüller, H.: Evaluation of MODIS columnar  
2 aerosol retrievals using AERONET in semi-arid Nevada and California, U.S.A., during the summer of 2012, *Atmos.*  
3 *Environ.*, 144, 345-360, 2016.

4 Lyapustin, A., Wang, Y., Laszlo, I., Kahn, R., Korkin, S., Remer, L., Levy, R., and Reid, J. S.: Multiangle  
5 implementation of atmospheric correction (MAIAC): 2. Aerosol algorithm, *J. Geophys. Res.*, 116, D03211,  
6 doi:10.1029/2010JD014986, 2011.

7 McLinden, C. A., Fioletov, V., Boersma, K. F., Krotov, N., Sioris, C. E., Veefkind, P., and Yang, K.: Air quality  
8 over the Canadian oil sands: A first assessment using satellite observations, *Geophys. Res. Lett.*, 39, L04804,  
9 <http://dx.doi.org/10.1029/2011GL050273>, 2012.

10 McLinden, C. A., Fioletov, V., Krotkov, N., Li, C., Boersma, K. F., and Adams, C.: A decade of change in NO<sub>2</sub> and  
11 SO<sub>2</sub> over the Canadian oil sands as seen from space, *Env. Sci. Tech.*, doi:10.1021/acs.est.5b04985, 2016.

12 Myhre, G., Shindell, D., Bréon, F.-M., Collins, W., Fuglestedt, J., Huang, J., Koch, D., Lamarque, J.-F., Lee, D.,  
13 Mendoza, B., Nakajima, T., Robock, A., Stephens, G., Takemura, T., and Zhang, H.: Anthropogenic and Natural  
14 Radiative Forcing. In: *Climate Change 2013: The Physical Science Basis. Contribution of Working Group I to the*  
15 *Fifth Assessment Report of the Intergovernmental Panel on Climate Change* [Stocker, T.F., D. Qin, G.-K. Plattner,  
16 M. Tignor, S.K. Allen, J. Boschung, A. Nauels, Y. Xia, V. Bex and P.M. Midgley (eds.)]. Cambridge University  
17 Press, Cambridge, United Kingdom and New York, NY, USA, 2013.

18 O'Neill, N. T., Eck, T. F., Holben, B. N., Smirnov, A., Royer, A., and Li, Z.: Optical properties of boreal forest fire  
19 smoke derived from Sun photometry, *J. Geophys. Res.*, 107, 4125, doi:10.1029/2001JD000877, 2002.

20 Popp, T., de Leeuw, G., Bingen, C., Brühl, C., Capelle, V., Chedin, A., Clarisse, L., Dubovik, O., Grainger, R.,  
21 Griesfeller, J., Heckel, A., Kinne, S., Klüser, L., Kosmale, M., Kolmonen, P., Lelli, L., Litvinov, P., Mei, L., North,  
22 P., Pinnock, S., Povey, A., Robert, C., Schulz, M., Sogacheva, L., Stebel, K., Zweers, D. S., Thomas, G., Tilstra, S.,  
23 Vandenbussche, L. G., Veefkind, P., Vountas, M. and Xue, Y.: Development, production and evaluation of aerosol  
24 Climate Data Records from European satellite observations (Aerosol\_cci), *Remote Sensing*, 8, 421,  
25 doi:10.3390/rs8050421, 2016.

26 Sayer, A. M., N. C. Hsu, C. Bettenhausen, and M.-J. Jeong (2013), Validation and uncertainty estimates for MODIS  
27 Collection 6 “Deep Blue” aerosol data, *J. Geophys. Res. Atmos.*, 118, 7864–7872, doi:10.1002/jgrd.50600.

28 Stieb, D. M., Burnett, R. T., Smith-Doiron, M., Brion, O., Shin, H. H., and Economou, V.: A New Multipollutant,  
29 No-Threshold Air Quality Health Index Based on Short-Term Associations Observed in Daily Time-Series  
30 Analyses, *J. Air & Waste Manage. Assoc.*, 58(3), 435-450, 2008.

31 Tian, J., and Chen, D.: Spectral, spatial, and temporal sensitivity of correlating MODIS aerosol optical depth with  
32 ground-based fine particulate matter (PM<sub>2.5</sub>) across southern Ontario, *Can. J. Remote Sensing*, 36, 119–128, 2010.

1 van Donkelaar, A., Martin, R. V., Brauer, M., Hsu, N. C., Kahn, R. A., Levy, R. C., Lyapustin, A., Sayer, A. M. and  
 2 Winker, D. M.: Global estimates of fine particulate matter using a combined geophysical-statistical method with  
 3 information from satellites, models, and monitors, *Environ. Sci. Technol.*, 50, 3762–3772, 2016.

4 Wu, A., Xiong, X., Doelling, D. R., Morstad, D., Angal, A., and Bhatt, R.: Characterization of Terra and Aqua  
 5 MODIS VIS, NIR, and SWIR spectral bands' calibration stability, *IEEE Trans. Geosci. Remote Sens.*, 51, 4330-  
 6 4338, 2013.

7  
 8

9 **Appendix A: Data product notes**

10 MODIS data is obtained from <ftp://ladsweb.nascom.nasa.gov/allData/>. AATSR and ATSR-2 version 4.1 data are  
 11 from Swansea University and can be obtained from the Aerosol CCI website (<http://www.esa-aerosol-cci.org/>)  
 12 following registration. The current file version (F12) is used for MISR  
 13 (<ftp://15eil01.larc.nasa.gov/MISR/MIL2ASAE.002>). The selected MISR AOD product is named the “regional best  
 14 estimate of spectral optical depth”. POLDER data was obtained from CNES (<http://polder.cnes.fr>), but data can  
 15 currently be obtained from <http://www.icare.univ-lille1.fr/> following registration. A POLDER AOD datum is  
 16 filtered if any of the following statements are true (see Bréon (2011)):

- 17 1) The central pixel is snow-covered.
- 18 2) One of the cloud tests is not applied.
- 19 3) None of the 9 radiance pixels which form the AOD superpixel has clear sky.
- 20 4) Sufficient data couples do not exist. The couples are:
  - 21 a) 865 nm & 910 nm,
  - 22 b) Q443 & U443,
  - 23 c) Q670 & U670,
  - 24 d) Q865 & U865,
  - 25 where Q and U are the derived Stokes elements and the number is the wavelength (in nm) of the  
 26 channel.
- 27 5) Ozone absorption is not corrected (using TOMS or ECMWF).
- 28 6) Stratospheric aerosol correction is uncertain or imprecise (i.e. stratospheric AOD larger than a certain  
 29 threshold).
- 30 7) Minimum scattering angle is larger than a threshold or maximum scattering angle is smaller than a  
 31 threshold.
- 32 8) Aerosol optical thickness is larger than a threshold such that surface reflectance cannot be estimated  
 33 adequately.
- 34 9) A large difference between measured and modeled reflectance exists for 443 nm.
- 35 10) Differences are too large between measured and modeled reflectance (risk of glitter).

- 1 11) Meteorological data indicate the presence of snow at ground level.
- 2 12) The quality index is 0.00 for viewing geometry conditions
- 3 13) The quality index is 0.00 for polarized reflectance fit.

4

5

6

7

8

9

10

11

12

13

14

15

16

17

18

19

20

21

22

23

24

Satellite	Time period	Wavelength (nm)	Spatial resolution of AOD superpixel at nadir (km <sup>2</sup> )	Spatial resolution of radiances (km <sup>2</sup> )
MISR	2000-2015	558	17.6 × 17.6	1.1 × 1.1
MODIS: Terra	2000-2015	470, 550, 660	10 × 10 (also 3 × 3)	0.25 × 0.25 to 1 × 1
Aqua	2002-2015			
POLDER: 1	1996-1997	865	18 × 21	6 × 7
2	2003			
(PARASOL) 3	2005-2013			
ATSR: ATSR-2	1995-2003	550	10 × 10	1 × 1
AATSR	2002-2012			

1  
2  
3  
4  
5  
6  
7  
8  
9  
10  
11  
12  
13  
14  
15  
16  
17  
18  
19  
20

**Table 1.** Spatial resolution of AOD data products from selected satellite instruments. The third column contains the wavelength at which aerosol optical depth is reported in each satellite data product. MISR and both MODIS instruments are currently operating.



Station name	lat(°N)	lon(°W)	Time span
Anzac	56.4493	-111.0372	2006-2015
Fort McMurray Athabasca Valley	56.7328	-111.39	1997-2015
Fort McMurray Patricia McInnes	56.7522	-111.476	1999-2015
Millenniummine	56.97	-111.4	2001-2015
Syncrude Upgrader Expansion 1	57.1492	-111.642	2002-2015
Fort McKay	57.1894	-111.641	1997-2015
Wapasu	57.2383	-110.9028	2013-2015
Shell Muskeg River	57.2491	-111.508567	2009-2015
Albian mine	57.2808	-111.526	2001-2009
Canadian Natural Resources Ltd. Horizon	57.3037	-111.739617	2008-2015

1  
2  
3  
4  
5  
6  
7  
8  
9  
10  
11  
12  
13  
14  
15  
16  
17  
18  
19  
20

**Table 2.** Selected NAPS PM<sub>2.5</sub> sites and time span of available data (inclusive)

AOD product	R	N
POLDER/PARASOL 865 nm	0.64	8
AATSR 550 nm	0.73	9
MISR 558 nm	0.20	10
MODIS/Aqua DT 550 nm	0.23	10
MODIS/Aqua DB 550 nm	0.57	10

1  
2  
3  
4  
5  
6  
7  
8  
9  
10  
11  
12  
13  
14  
15  
16  
17  
18  
19  
20  
21  
22

**Table 3.** Spatial correlation between PM<sub>2.5</sub> mass density and AOD using medians of coincident data at 10 sites in the AOSR. Wapasu has insufficient or no temporal overlap with POLDER/PARASOL and AATSR. Syncrude UE1 is not spatially coincident with any of the POLDER locations given the 10 km criterion (see Sect. 2).

sensor	$r_s$	slope	offset	seasonal $r$	month range	N
Aqua DB v6	0.793	0.867	0.0233	0.84	4-10	5508
	0.686	1.013	0.0036	0.84	4-10	626
Aqua DT v6	0.875	1.210	-0.0117	0.99	4-10	4197
	0.806	1.088	-0.0223	0.95	5-9	431
PARASOL	0.867	0.831	-0.018	0.89	5-10	414
	-	-	-	-	-	-
AATSR	0.888	0.862	0.0253	0.96	5-10	560
	-	-	-	-	-	-
MISR	0.862	0.731	0.0219	0.88	3-9	337
	0.668	0.652	0.032	-	-	87

1  
2  
3  
4  
5  
6  
7  
8  
9  
10  
11  
12  
13  
14  
15  
16  
17  
18

**Table 4.** Statistical comparison of coincident AODs observed by satellite-based sensors and AERONET Cimel sun photometers. For each satellite AOD product, the upper row is for Fort McMurray and the lower row is for Fort McKay. The Cimel 500 nm AOD, scaled to the satellite AOD wavelength (see Sect. 2), is used for comparison with all satellite sensors except POLDER/PARASOL, for which the Cimel 870 nm AOD is more appropriate (see Table 1). The number of MISR-Fort McKay coincidences is insufficient to assess the month-to-month variability.

	Including +4 $\sigma$ outliers	Excluding +4 $\sigma$ outliers
POLDER/PARASOL	0.995	0.81
MISR	0.91	0.94
AATSR	0.98	0.92
MODIS DT	0.98	0.94
MODIS DB	0.91	0.86

1

2 **Table 5.** Correlation of annual mean AODs with Fort McMurray AERONET AODs during the respective overlap  
3 periods of the various satellite AOD products. In the rightmost column, the contribution of large forest fires has been  
4 removed from AERONET data and satellite datasets using +4 standard deviations ( $\sigma$ ) as a cutoff.

5

6

7

8

9

10

11

12

13

14

15

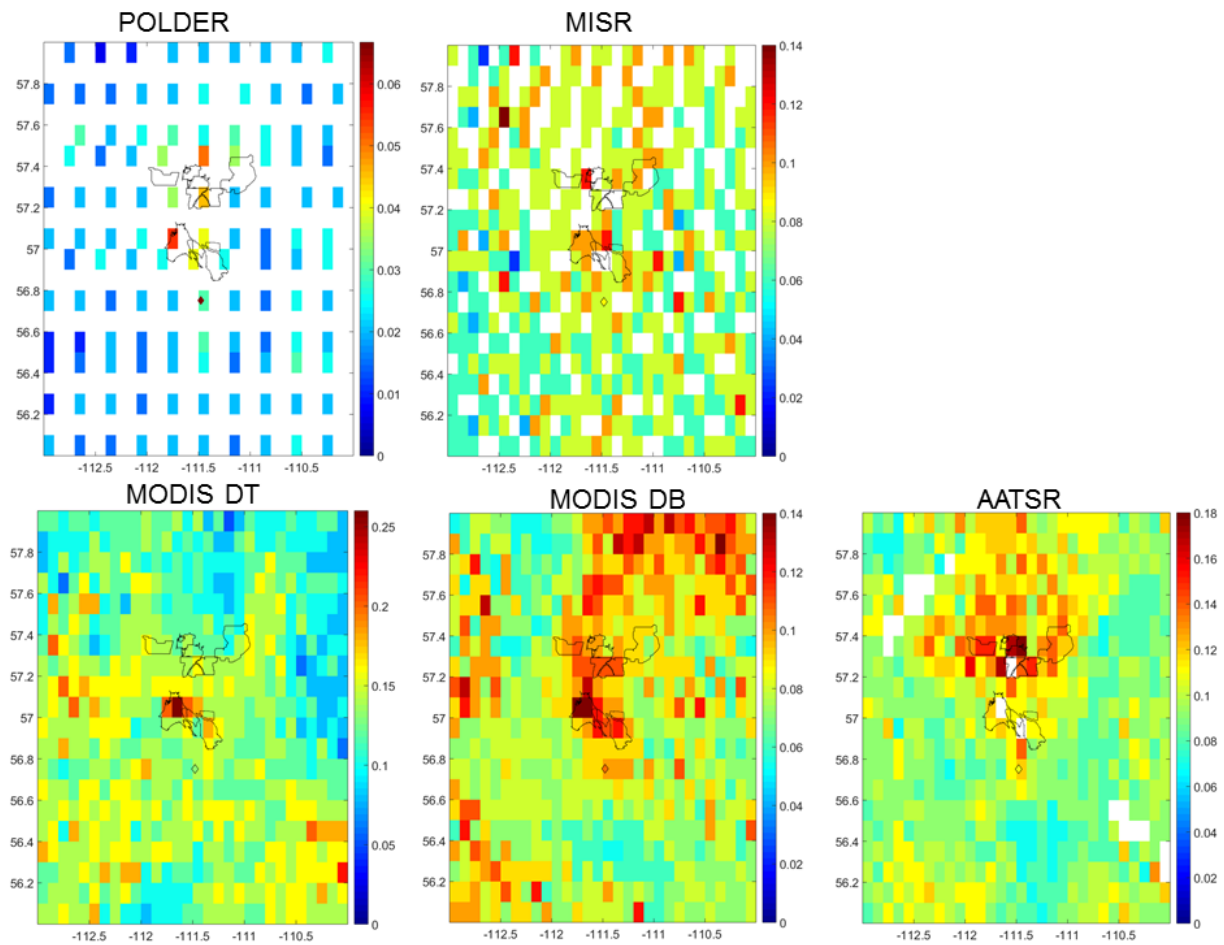
16

17

18

19

20



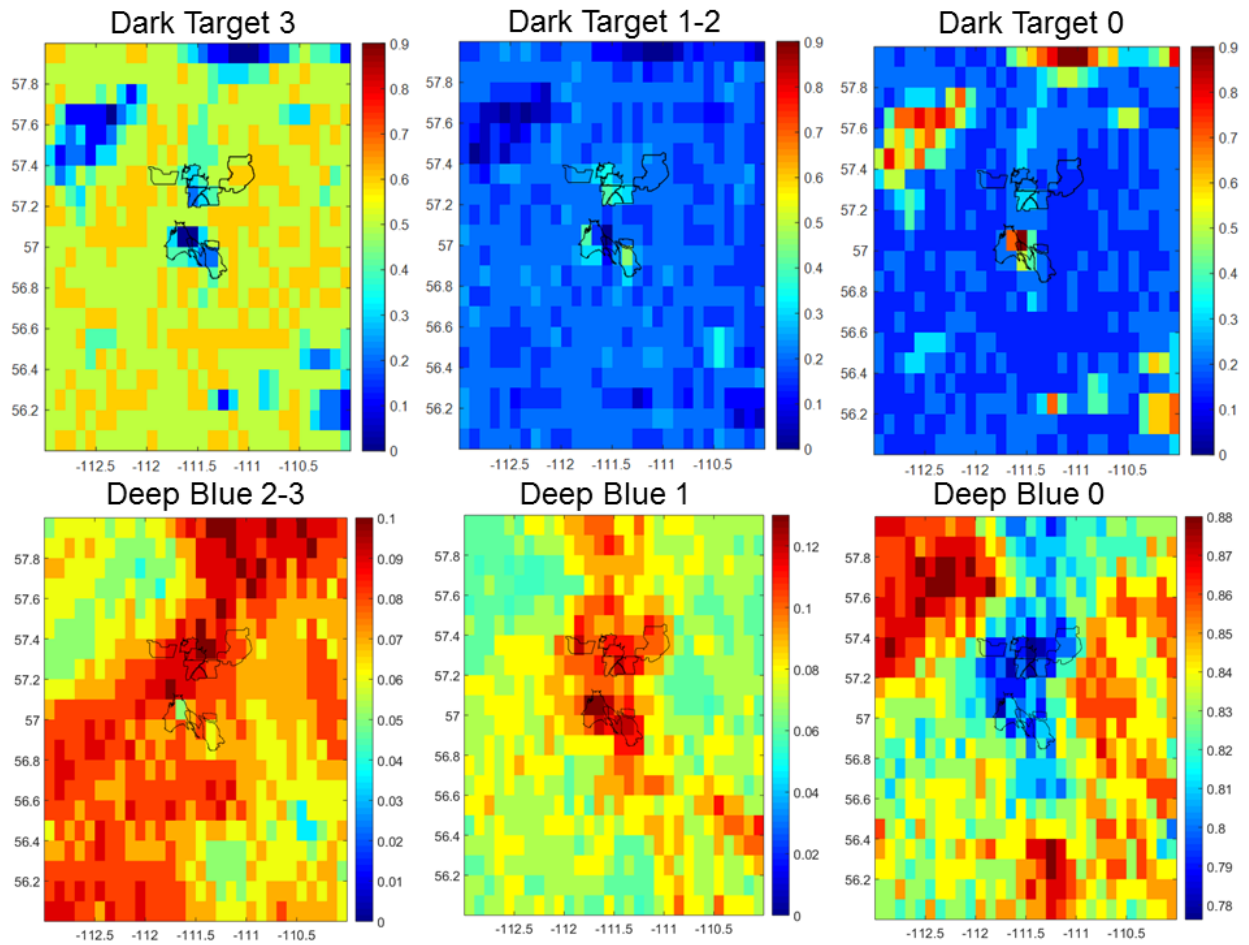
1  
 2 **Figure 1.** Climatological average AOD maps on a  $0.1^\circ \times 0.1^\circ$  latitude-longitude grid. (top left) POLDER 865 nm  
 3 (1996-2013). Note the gaps in time between the different members of the POLDER series in Table 1. (top right)  
 4 MISR 558 nm (2000-2015). (bottom left) MODIS/Aqua DT using only confidence of 3 (2002-2015). (bottom  
 5 centre) MODIS/Aqua DB using only confidences of 2-3 (2002-2015) following Sayer et al., 2013. (bottom right)  
 6 AATSR 550 nm (2002-2012). Typical N is  $\sim 65$  for AATSR (see below) and white areas indicate  $N < 20$ . Black lines  
 7 trace out the three surface mining areas in this and subsequent figures. A average coincident AERONET AOD at Fort  
 8 McMurray is superimposed as a diamond with a black outline. In each panel, the AOD ranges from 0 to the greater  
 9 of the maximum climatological mean satellite AOD or the Fort McMurray AERONET mean AOD, except for  
 10 MISR, for which the AOD range is capped at 0.14 to not emphasize the anomalously high AOD at Moose Lake  
 11 ( $57.6^\circ\text{N}$ ,  $112.5^\circ\text{W}$ ).

12  
 13  
 14  
 15

1

2

3



4

5 **Figure 2.** Maps of fraction of pixels with a specific confidence (2002-2014) for MODIS/Aqua DT (top) and DB  
 6 (bottom) AODs. Lower confidence is expected over Moose Lake and the Richardson sand dunes (58.0°N, 111.0°W).  
 7 MODIS DB only reports a fill value when confidence is 0 in contrast to MODIS DT, thus the bottomright plot  
 8 accounts for fill values, whereas the topright plot (for MODIS DT) does not.

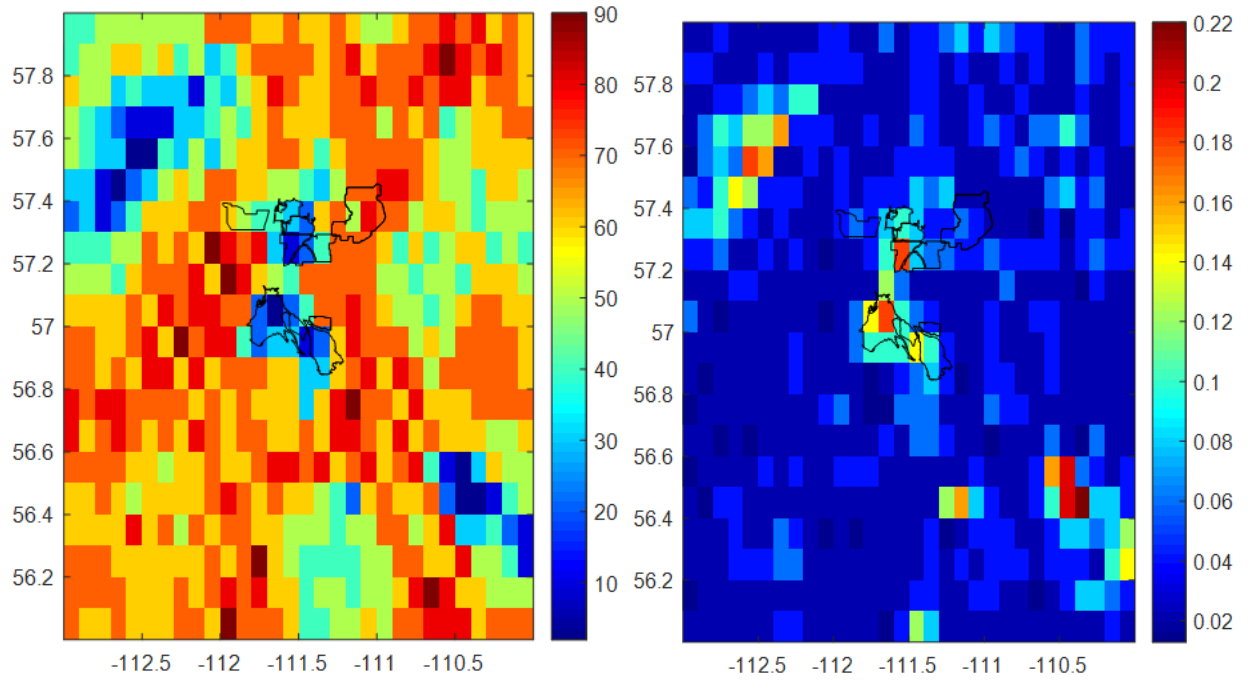
9

10

11

12

13



1

2

3

4

5

6

7

8

9

10

11

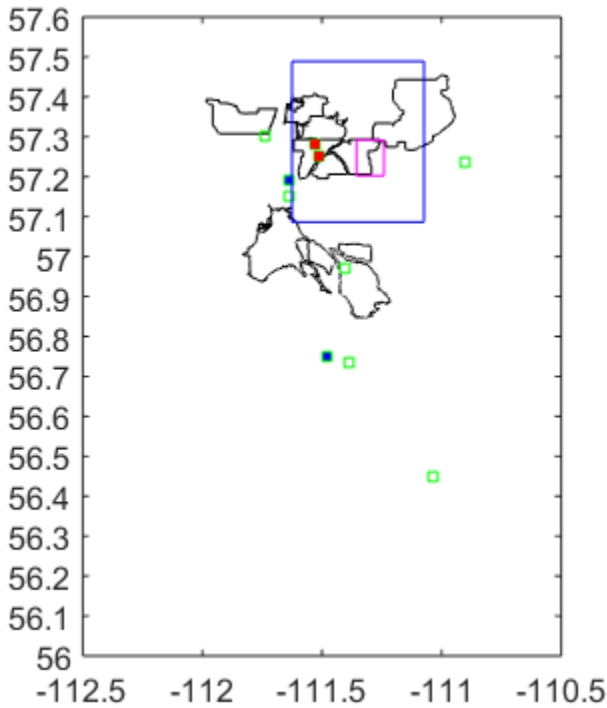
12

13

14

15

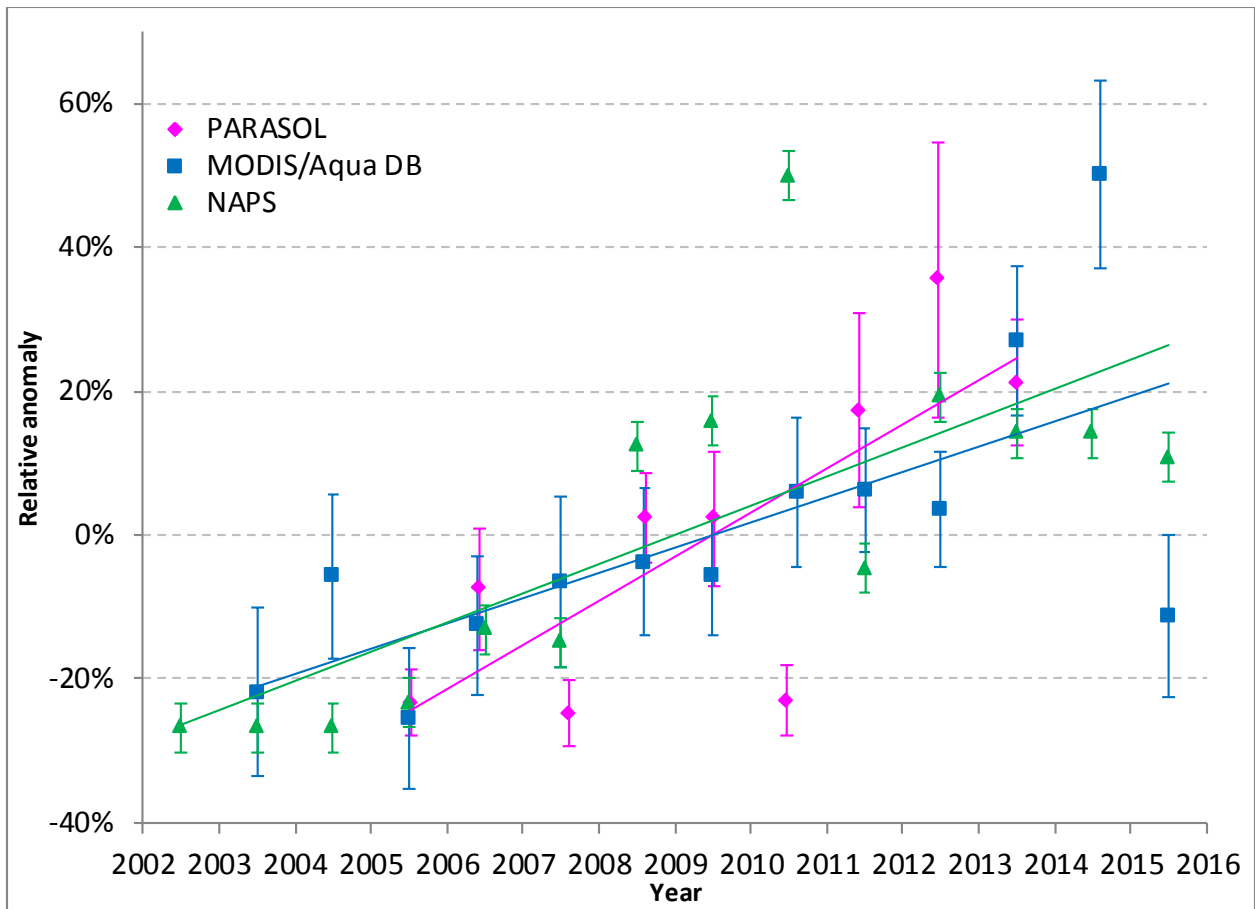
**Figure 3.** Map of sample size (left) and average cloud fraction within AOD superpixels when the AOD retrieval is successful (right), compiled from the entire AATSR data record. Smaller sample sizes are expected over Moose Lake and Gordon Lake (56.5°N, 110.5°W).



1  
 2 **Figure 4.** Areas with a significant positive trend in AOD in the POLDER/PARASOL, and MODIS/AquaDB data  
 3 records. The area over which the AOD time series is determined for MODIS/Aqua DB ( $0.1 \times 0.1^\circ$ ), and  
 4 POLDER/PARASOL ( $0.4 \times 0.4^\circ$ ) is outlined in pink and blue, respectively. Locations of 10 NAPS  $PM_{2.5}$  monitoring  
 5 sites are also shown as small green squares. The central one of 3 adjacent (overlapping) grid cells at constant latitude  
 6 is plotted for POLDER/PARASOL (see Sect. 3 for details). The grid cell with the largest trend in the domain is  
 7 plotted for MODIS/AquaDB (see Sect. 3 for details). Note that the Albian mine site ( $57.2808^\circ\text{N}$ ,  $111.526^\circ\text{W}$ ) was  
 8 replaced by the nearby Shell Muskeg River site ( $57.2491^\circ\text{N}$ ,  $111.509^\circ\text{W}$ ) in 2009 (both station symbols are filled in  
 9 red). The two AERONET instruments are co-located with NAPS monitors and those sites are filled in blue.

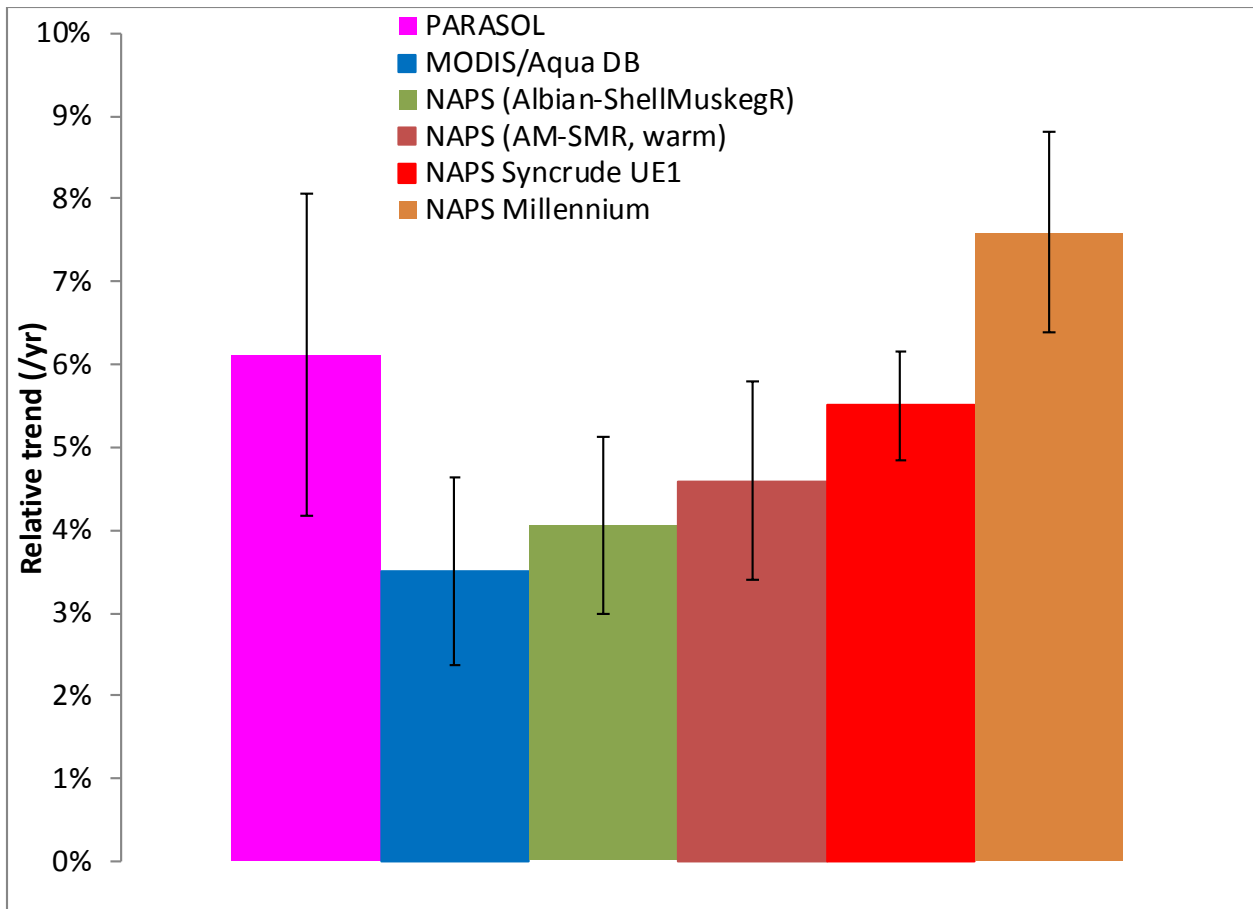
10  
 11  
 12





1  
2 **Figure 5.** Relative anomalies of annual mean PM<sub>2.5</sub> mass density for the merged Albion mine and Shell Muskeg  
3 River dataset, along with relative anomalies of bias-corrected annual mean AODs for POLDER/PARASOL and  
4 MODIS/Aqua DB (see Sect. 3 for details and Fig. 4 for satellite trend areas). Each satellite time series is plotted at  
5 the average decimal time for each calendar year. Trend lines are fitted to each time series using a matching colour.  
6 Vertical error bars indicate  $\pm 1$  relative standard error of the annual mean. There are, on average, 33 and 50  
7 observations per year for POLDER/PARASOL and MODIS/Aqua DB, respectively.

8  
9  
10  
11



1  
 2 **Figure 6.** Relative trend in annually averaged PM<sub>2.5</sub> mass density calculated using NAPS PM<sub>2.5</sub> data for three  
 3 locations, namely the merged Albian mine and Shell Muskeg River dataset (2002-2015), Millennium mine (2002-  
 4 2014) and Syncrude UE1 (2003-2014), or in satellite AODs in the vicinity of Shell’s Albian and Muskeg River  
 5 mines (see Fig. 4 and Sect. 3). The trend is also determined for the NAPS PM<sub>2.5</sub> merged Albian Mine – Shell  
 6 Muskeg River (AM-SMR) dataset limiting to the warm season (April to October). Trend uncertainty is indicated  
 7 with a vertical bar (±1 s. e.).